LIMNOLOGY
AND
OCEANOGRAPHY

December 2001
Volume 46
Number 8

Limnol. Oceanogr., 46(8), 2001, 1845–1859

Seasonal dynamics of coastal ecosystems and export production at high latitudes: A modeling study

Ru Cheng Tian[1], *Alain F. Vézina*[2], *Michel Starr, and François Saucier*
Ocean Sciences Division, Maurice Lamontagne Institute, C.P. 1000, Mont-Joli, Quebec G5H 3Z4, Canada

Abstract

Export of organic matter from the surface to deeper waters often shows much smaller seasonal variations than primary production or nitrate-based new production in mid- to high-latitude marine systems. The mechanisms underlying this pattern remain poorly understood, but seasonal shifts in food web structure and dynamics have been implicated. We report here on an ecosystem modeling analysis of a high-resolution (biweekly) time series of biomass, production, and export flux (sediment trap) measurements conducted in 1991 in Bonne Bay (Newfoundland). This time series shows the classical pattern of a spring bloom followed by a summer low biomass period, yet export is bimodal, with maxima during spring and late summer. The ecosystem model was forced by diagnostic vertical mixing calculations based on temperature and salinity records taken every 3 d and hourly wind data. The physical analysis indicated that the nitrate flux into the euphotic zone during summer was equivalent to that during the spring and fall seasons and accounted for half of the summer export. Statistical adjustments of the parameters of the ecosystem model indicated that strong production of dissolved organic carbon during the spring bloom, high temperature dependence of microbial activity, and physico-chemical particle aggregation played key roles in explaining the remainder of the summer export. Seasonal changes in trophic pathways between spring and summer, such as a shift from a herbivorous to a microbial food web, played a comparatively smaller role. Our modeling analysis suggests that physical mixing processes and physico-chemical aggregation processes are at least as important as shifts in food web trophic pathways in explaining the postbloom export flux in mid- to high-latitude marine systems.

The export of photosynthetically fixed carbon in surface waters to deeper waters is a fundamental process in planktonic ecosystems that influences atmospheric-ocean carbon flux (Falkowski et al. 1998) and supplies energy and nutrients to deep-water and benthic food webs (Graf 1992). This export, assumed to be largely in the form of sinking particles, is generally associated with periods when nutrients are abundant and when food chains are short and dominated by large phytoplankton and herbivorous zooplankton (Michaels and Silver 1988; Boyd and Newton 1995). In contrast, periods when nutrients are scarce and when complex microbial food webs dominate are believed to be more efficient at recycling and are generally associated with low export. Temperate and high-latitude marine ecosystems are strongly influenced by the seasonal cycle of stratification of the upper ocean, leading to a nutrient-rich spring bloom period followed by a nutrient-poor summer stratified period. Export fluxes should be higher during the spring bloom, dominated by large-sized herbivorous food webs, than during summer when the microbial food web prevails.

Recent evidence, however, does not always agree with this conceptual model. Export fluxes, once normalized to surface production (export ratios), do not show evident control by surface production and food web structure, both in open ocean (Karl et al. 1996) and coastal systems (Olesen and Lundsgaard 1995). Smith and Dunbar (1998), working in the Ross Sea, have demonstrated significant lags between new production and blooms on one hand and export fluxes on the other. They suggested that variability in heterotrophic remineralization may be involved in these lags. Rivkin et al. (1996), working in the subarctic Gulf of St. Lawrence, have shown that there is no relationship between export fluxes and seasonal shifts in new production and food web structure: export fluxes were just as high postbloom as during the spring bloom. They attributed this to the replacement of the large phytoplankton size class dominant during spring by the

[1] To whom correspondence should be addressed. Present address: Ocean Sciences Centre, Memorial University of Newfoundland, St. John's, Newfoundland, Canada A1C 5S7 (rtian@morgan.ucs.mun.ca).
[2] Present address: Bedford Institute of Oceanography, 1 Challenger Drive, Dartmouth, Nova Scotia, Canada B2Y 4A2.

Acknowledgements

This work was supported financially by the Ocean Climate Program of the Department of Fisheries and Oceans, Canada, and by a NSERC research grant to A.F.V.

Table 1. State variables of the ecosystem model (units are that of final outputs after N-C conversion).

Symbol	Variable	Value (unit)
Bac	Bacteria	(mg C m^{-3})
DOC	Dissolved organic carbon	(mg C m^{-3})
LP	Large sinking particles	(mg C m^{-3})
Mez	Mesozooplankton	(mg C m^{-3})
Miz	Microzooplankton	(mg C m^{-3})
NH_4^+	Ammonium	(μM)
NO_3^-	Nitrate	(μM)
Pl	Large phytoplankton (>5 μm)	(mg C m^{-3})
Ps	Small phytoplankton (<5 μm)	(mg C m^{-3})
SP	Small detrial particles	(mg C m^{-3})

microzooplankton size class during summer. The microzooplankton essentially substituted for the large phytoplankton, sustaining the mesozooplankton and maintaining total flux through an increased contribution of fecal pellets. Thus, in this model, the shift in food web structure acts to decrease the variability in export flux throughout the growing season, not increase the variability as in the classical view.

To distinguish between these alternatives, we need more work on relating production, food web structure, remineralization, and export over seasonal scales. Ecosystem modeling is well suited to explore how processes interact across time and space to generate observed patterns. Here we present an ecosystem modeling study of a time series gathered during 1991 in Bonne Bay, a deep subarctic fjord on the western shore of Newfoundland (Starr et al. 1994). The observations in that system indicate a bimodal pattern in vertical flux, with maxima during the spring bloom and in late summer, that contrasts with a single spring peak in phytoplankton biomass. This generally concurs with what was reported by Rivkin et al. (1996) for the adjacent Gulf of St. Lawrence (GSL). The difference is that this time series provides us with a much denser set of observations (biweekly) to examine the relationship between production and export.

The model is one-dimensional and ignores lateral advective effects on physical and biological properties. We consider this an adequate approximation for most of the time series because runoff to the fjord is low and exchange processes with the GSL are weak and intermittent (Gilbert and Pettigrew 1993). The ecosystem model spans both the herbivorous diatom-copepod food chain and the microbial food web (Tian et al. 2000) and is driven by a diagnostic vertical mixing model based on temperature and salinity profiles collected every 3 d and hourly wind forcing. High resolution in time (hourly) and depth (1 m) was adopted to capture as realistically as possible the fluctuations in the physical processes that can influence the relationship between production and export. Parameter estimation techniques were used to objectively minimize the discrepancies between model and data. The minimization process was repeated from different initial parameter values, and the results were used to identify the most critical parameters and the mechanisms underlying the production-export relationship.

Table 2. Definition of symbols used in Table 3 (model equations) including model parameters.

Parameter description		Units
α_{AN}	Nitrification rate	d^{-1}
α_f	Aggregation coefficient	m^3 mg C^{-1}
α_{kzc}	Convection-mixed layer depth relation	
α_{MezDOC}	DOC from feeding losses of mesozooplankton	%
α_{MezSP}	Small particles from feeding losses of Mez	%
α_{MizSP}	Small particles from feeding losses of Miz	%
α_{PlDOC}	DOC production of large phytoplankton	%
α_{PsDOC}	DOC production of small phytoplankton	%
$\beta_{T\mathrm{Bac}}$	Constant of T influence on bacterial growth	
$\beta_{T\mathrm{Miz}}$	Constant of T influence on MiZ growth	
$\beta_{T\mathrm{Mez}}$	Constant of T influence on Mez growth	
β_{TP}	Constant of T influence on P_l (P_s) growth	
bac_f	Fraction of free bacteria	%
$\mathrm{C:Chl}a_{\mathrm{Pl}}$	C : Chlorophyl *a* in large phytoplankton	
$\mathrm{C:Chl}a_{\mathrm{Ps}}$	C : Chlorophyl *a* in small phytoplankton	
c_{LPSP}	Breakdown coefficient of large particles	d^{-1}
e_{Bac}	Growth efficiency of bacteria	%
e_{MezMiz}	Growth efficiency of Mez predation on Miz	%
e_{MezPl}	Growth efficiency of Mez grazing on Pl	%
e_{MizBac}	Growth efficiency of Miz grazing on Bac	%
e_{MizPs}	Growth efficiency of Miz grazing on Ps	%
e_{MizPs}	Growth efficiency of Miz grazing on SP	%
g_{Mez0}	Maximum mesozooplankton grazing rate at 0°C	d^{-1}
$g_{\mathrm{Mez}}(T)$	Temperature-dependent mesozooplankton grazing rate	d^{-1}
g_{Miz0}	Maximum microzooplankton grazing rate at 0°C	d^{-1}
$g_{\mathrm{Miz}}(T)$	Temperature-dependent microzooplankton grazing rate	d^{-1}
H_{BacDOC}	Half saturation of DOC for bacteria	mg C m^{-3}
H_{BacSP}	Half saturation of small particles for bacteria	mg C m^{-3}
H_{MezLP}	Half saturation of large particles for Mez	mg C m^{-3}
H_{MezMiz}	Half saturation of Mez predation on Miz	mg C m^{-3}
H_{MezPl}	Half saturation of Mez grazing on Pl	mg C m^{-3}
H_{MizBac}	Half saturation of Miz predation on Bac	mg C m^{-3}
H_{MizPs}	Half saturation of Miz grazing on Ps	mg C m^{-3}
H_{MizSP}	Half saturation of small particles for Miz	mg C m^{-3}
$H_{\mathrm{Pl}A}$	Half saturation of NH_4^+ for P_l	μM
$H_{\mathrm{Pl}N}$	Half saturation of NO_3^- for P_l	μM
$H_{\mathrm{Ps}A}$	Half saturation of NH_4^+ for P_s	μM
$H_{\mathrm{Ps}N}$	Half saturation of NO_3^- for P_s	μM
$K(z)$	Diffusion coefficient	m^2 d^{-1}
m_{Bac}	Bacterial mortality and excretion	d^{-1}
m_{MezLP}	Mortality of mesozooplankton	d^{-1}
m_{PlLP}	Mortality of large phytoplankton	%
μ_{Bac0}	Maximum bacterial uptake rate at 0°C	d^{-1}
$\mu_{\mathrm{Bac}}(T)$	Temperature-dependent bacterial uptake rate	d^{-1}
μ_{Pl0}	Maximum growth rate of large phytoplankton at 0°C	d^{-1}
μ_{Pl}	Actual growth rate of large phytoplankton	d^{-1}
$\mu_{\mathrm{Pl}}(N)$	Nutrient-limited large phytoplankton growth rate	d^{-1}
μ_{Ps0}	Maximum growth rate of small phytoplankton at 0°C	d^{-1}
μ_{Ps}	Actual growth rate of small phytoplankton	d^{-1}
$\mu_{\mathrm{Ps}}(N)$	Nutrient-limited small phytoplankton growth rate	d^{-1}
$r_{\mathrm{Mez}A}$	NH_4^+ from mesozooplankton respiration	%
$r_{\mathrm{Miz}A}$	NH_4^+ from microzooplankton respiration	%
s	Sinking velocity of large particles	m d^{-1}
u	Current velocity	m d^{-1}
z	Depth in water column	m

Modeling methodology

Ecosystem model—The ecosystem model is described in detail in a previous paper (Tian et al. 2000) that reports an analysis of a JGOFS (Joint Global Ocean Flux Study) data set. We briefly go over the major features of the model and describe in more depth modifications from the original version. A simple prescribed seasonal mixed layer with constant eddy diffusivity within and below the mixed layer was used in the original version, whereas here the vertical mixing coefficients vary continuously with depth and respond to variations in the wind stress. Temperature forcing on biological rates and parameter estimation to optimize the fit between simulations and observations were implemented as well. All model state variables, parameters, and equations are documented in Tables 1–3.

The model includes ten state variables (Table 1), including a large-sized herbivorous food chain (nitrate, large phytoplankton [>5 μm], mesozooplankton [>0.2 μm], and large sinking particles) and the microbial food web (ammonium, small phytoplankton [<5 μm], microzooplankton [<0.2 μm], small suspended particles, dissolved organic matter, and bacteria). The basic unit of the model is nitrogen, but the results are expressed in carbon units through multiplication by the Redfield ratio (C : N = 6.625 in moles) to facilitate comparisons with the data.

The phytoplankton growth rates are forced by PAR (photosynthetically available radiation), nitrogenous nutrients, and temperature. Limitation by PAR is given by

$$\mu(\mathrm{PAR}) = P_m(1 - e^{-\alpha \mathrm{PAR}/P_m})e^{-\beta \mathrm{PAR}/P_m} \tag{1}$$

where μ(PAR) is the light-limited growth rate (d^{-1}), P_m is the maximum biomass-normalized gross photosynthetic rate (d^{-1}), α is the initial slope of photosynthesis-irradiance relationship (0.08 W^{-1} d^{-1}), and β is the photoinhibition coefficient (0.001 W^{-1} d^{-1}; Platt et al. 1980). Both photosynthetic parameters imply a carbon-to-chlorophyll ratio of 50. Limitation by nitrogenous nutrients is given by

$$\mu_{\mathrm{Pl}}(N) = \frac{\mathrm{NH}_4^+}{\mathrm{NH}_4^+ + H_{\mathrm{Pl}A}} + \frac{\mathrm{NO}_3^-}{\mathrm{NO}_3^- + H_{\mathrm{Pl}N}} \times \frac{H_{\mathrm{Pl}A}}{\mathrm{NH}_4^+ + H_{\mathrm{Pl}A}} \tag{2}$$

where $\mu_{\mathrm{Pl}}(N)$ (or $\mu_{\mathrm{Ps}}(N)$) is the large (or small) phytoplankton relative nutrient-limited growth rate; $H_{\mathrm{Pl}N}$ and $H_{\mathrm{Pl}A}$ are the half-saturation constants for NO_3^- and NH_4^+ uptake (μM) by large phytoplankton (or $H_{\mathrm{Ps}N}$ and $H_{\mathrm{Ps}A}$ for small phytoplankton), respectively (Parker 1993). Finally, limitation by temperature is given by

$$\mu_{\mathrm{Pl}}(T) = \mu_{\mathrm{Pl}0}e^{\beta_{TP}T} \tag{3}$$

where T is the temperature in the surface mixed layer; $\mu_{\mathrm{Pl}0}$ (or $\mu_{\mathrm{Ps}0}$) is the large (or small) phytoplankton maximum growth rate at 0°C (d^{-1}); and β_{TP} is the exponent of the temperature-dependence of phytoplankton growth rate (Verity 1981). The phytoplankton growth rate is computed as the product of these three terms

$$\mu_{\mathrm{Pl}} = \mu(\mathrm{PAR})\mu_{\mathrm{Pl}}(N)\mu_{\mathrm{Pl}}(T)$$
$$(\text{or } \mu_{\mathrm{Ps}} = \mu(\mathrm{PAR})\mu_{\mathrm{Ps}}(N)\mu_{\mathrm{Ps}}(T)) \tag{4}$$

Mesozooplankton consume large phytoplankton, microzooplankton, and large particles, whereas microzooplankton feed on small phytoplankton, bacteria, and small particles. The specific feeding rate of a predator j on food type i is calculated as

$$G_j^i = \frac{g_j c_i F_i}{1 + F_t}, \quad \text{with } F_t = \sum c_i F_i \tag{5}$$

where g_j is the maximum grazing rate; c_i is the food preference (inverse of the half-saturation constants), and F_t is the total food (Fasham et al. 1999). Compared with the previous version of the model where both preference coefficients and half-saturation constants to describe prey selection were used, this formulation reduces the number of model parameters to estimate. Temperature influence upon zooplankton grazing and bacterial uptake rates is parameterized by an exponential law as for phytoplankton (Huntley and Lopez 1992).

Large particles are a mixture of fecal pellets, aggregates, and dead bodies, whereas small particles are formed through feeding losses. Aggregation fluxes of suspended particles (Φ_f: mg C m^{-3} d^{-1}) are related to current shear in the water column and the square of the concentration of small particles (SP) and small phytoplankton (Ps)

$$\Phi_f = \alpha_f \frac{\partial u}{\partial z}(Ps^2 + SP^2) \tag{6}$$

where α_f is the aggregation coefficient, u is the current velocity, and z is the depth. Other mechanisms such as differential sedimentation and Brownian motion are not explicitly parameterized (Jackson 1990). These processes are linked to particle concentrations so that Eq. 6 can partly represent the effect of these mechanisms. Remineralization of dissolved organic matter (DOM) and small detritus through bacterial action is parameterized as a function of substrate concentration corrected for threshold concentrations of refractory materials. Regenerated ammonium from bacterial and zooplankton respiration is either taken up by phytoplankton in the euphotic zone or nitrified throughout the water column. Nitrification rate is parameterized as a function of light intensity due to photoinhibition in surface waters. Downward fluxes are determined by large particle sinking (F_{LP}) and detrainment (F_X)

$$F_{\mathrm{LP}} = s\frac{\partial \mathrm{LP}}{\partial z} \quad \text{and} \quad F_X = K(z)\frac{\partial X}{\partial z} \tag{7}$$

where s is the particle sinking velocity, $K(z)$ is the turbulent eddy diffusivity (following section), and X represents all organic carbon pools.

Physical forcing—The turbulent eddy diffusivity, $K(z)$, is computed by a diagnostic model following Denman and Gargett (1983) and Yoshida and Oakey (1996)

$$K(z) = A\varepsilon\left(\frac{g\partial\rho_w}{\rho\partial z}\right)^{-1} \tag{8}$$

with

$$\varepsilon = \varepsilon_w + \varepsilon_c; \qquad \varepsilon_w = \frac{\omega_*^3}{kz} \quad \text{and} \quad \varepsilon_c = 7.5\nu\left(\frac{\partial u}{\partial z}\right)^2$$

Table 3. Model equations. State variables are defined in Table 1 and other symbols, including model parameters, are defined in Table 2.

Herbivorous food web

$$\frac{\partial Pl}{\partial t} = \mu_{\mathrm{Pl}} Pl - (m_{\mathrm{PlLP}} + \alpha_{\mathrm{PlDOC}})Pl - \frac{g_{\mathrm{Mez}}(T)\mathrm{Mez}Pl/H_{\mathrm{MezPl}}}{1 + F_{tl}} + \frac{\partial}{\partial z}\left[K(z)\frac{\partial Pl}{\partial z}\right]$$

where $F_{tl} = Pl/H_{\mathrm{MezPl}} + \mathrm{Miz}/H_{\mathrm{MezMiz}} + \mathrm{LP}/H_{\mathrm{MezLP}}$

$$\frac{\partial \mathrm{Mez}}{\partial t} = g_{\mathrm{Mez}}(T)\mathrm{Mez}\frac{e_{\mathrm{MezPl}}Pl/H_{\mathrm{MezPl}} + e_{\mathrm{MezMiz}}\mathrm{Miz}/H_{\mathrm{MezMiz}} + e_{\mathrm{MezLP}}\mathrm{LP}/H_{\mathrm{MezLP}}}{1 + F_{tl}} - m_{\mathrm{MezLP}}\mathrm{Mez} + \frac{\partial}{\partial z}\left[K(z)\frac{\partial \mathrm{Mez}}{\partial z}\right]$$

$$\frac{\partial \mathrm{LP}}{\partial t} = g_{\mathrm{Mez}}(T)\mathrm{Mez}\frac{f_{\mathrm{PlLP}}Pl/H_{\mathrm{MezPl}} + f_{\mathrm{Miz}}\mathrm{Miz}/H_{\mathrm{MezMiz}} + f_{\mathrm{LP}}\mathrm{LP}/H_{\mathrm{MezLP}}}{1 + F_{tl}} + m_{\mathrm{PlLP}}Pl + m_{\mathrm{MezLP}}\mathrm{Mez} + \alpha_f\frac{\partial u}{\partial z}(Ps^2 + \mathrm{SP}^2)$$
$$- g_{\mathrm{Mez}}(T)\mathrm{Mez}\frac{\mathrm{LP}/H_{\mathrm{MezLP}}}{1 + F_{tl}} - c_{\mathrm{LPSP}}\mathrm{LP} + \frac{\partial}{\partial z}\left[K(z)\frac{\partial \mathrm{LP}}{\partial z}\right] - s\frac{\partial \mathrm{LP}}{\partial z}$$

where $f_{(\mathrm{Pl,Miz,LP})} = 1 - \alpha_{\mathrm{MezDOC}} - \alpha_{\mathrm{MezSP}} - r_{\mathrm{MezA}} - (e_{\mathrm{MezPl}}, e_{\mathrm{MezMiz}}, e_{\mathrm{MezLP}})$

Microbial food web

$$\frac{\partial Ps}{\partial t} = \mu_{\mathrm{Ps}}Ps - \frac{g_{\mathrm{Miz}}(T)\mathrm{Miz}Ps/H_{\mathrm{MizPs}}}{1 + F_{ts}} - \alpha_{\mathrm{PsDOC}}Ps - \alpha_f\frac{\partial u}{\partial z}Ps^2 + \frac{\partial}{\partial z}\left[K(z)\frac{\partial Ps}{\partial z}\right]$$

where $F_{ts} = Ps/H_{\mathrm{MizPs}} + \mathrm{Bac}/H_{\mathrm{MizBac}} + \mathrm{SP}/H_{\mathrm{MizSP}}$

$$\frac{\partial \mathrm{Miz}}{\partial t} = g_{\mathrm{Miz}}(T)\mathrm{Miz}\frac{e_{\mathrm{MizPs}}Ps/H_{\mathrm{MizPs}} + e_{\mathrm{MizBac}}\mathrm{Bac}/H_{\mathrm{MizBac}} + e_{\mathrm{MizSP}}\mathrm{SP}/H_{\mathrm{MizSP}}}{1 + F_{ts}} - g_{\mathrm{Mez}}(T)\mathrm{Mez}\frac{\mathrm{Miz}/H_{\mathrm{MezMiz}}}{1 + F_{tl}} + \frac{\partial}{\partial z}\left[K(z)\frac{\partial \mathrm{Miz}}{\partial z}\right]$$

$$\frac{\partial \mathrm{SP}}{\partial t} = c_{\mathrm{LPSP}}\mathrm{LP} + g_{\mathrm{Mez}}(T)\alpha_{\mathrm{MezSP}}\mathrm{Mez}\frac{F_{tl}}{1 + F_{tl}} + g_{\mathrm{Miz}}(T)\alpha_{\mathrm{MizSP}}\mathrm{Miz}\frac{F_{ts}}{1 + F_{ts}} - g_{\mathrm{Miz}}(T)\mathrm{Miz}\frac{\mathrm{SP}/H_{\mathrm{MizSP}}}{1 + F_{ts}} - \mu_{\mathrm{Bac}}(T)\mathrm{Bac}\frac{(1 - \mathrm{bac}_f)(\mathrm{SP} - T_{\mathrm{BacSP}})}{\mathrm{SP} - T_{\mathrm{BacSP}} + H_{\mathrm{BacSP}}}$$
$$- \alpha_f\frac{\partial u}{\partial z}\mathrm{SP}^2 + \frac{\partial}{\partial z}\left[K(z)\frac{\partial \mathrm{SP}}{\partial z}\right]$$

$$\frac{\partial \mathrm{DOC}}{\partial t} = g_{\mathrm{Mez}}(T)\alpha_{\mathrm{MezDOC}}\mathrm{Mez}\frac{F_{tl}}{1 + F_{tl}} + g_{\mathrm{Miz}}(T)\mathrm{Miz}\frac{\alpha_{\mathrm{Ps}}Ps/H_{\mathrm{MizPs}} + \alpha_{\mathrm{Bac}}\mathrm{Bac}/H_{\mathrm{MizBac}} + \alpha_{\mathrm{SP}}\mathrm{SP}/H_{\mathrm{MizSP}}}{1 + F_{ts}} + \alpha_{\mathrm{PlDOC}}Pl + \alpha_{\mathrm{PsDOC}}Ps$$
$$- \mu_{\mathrm{Bac}}(T)\mathrm{Bac}\frac{\mathrm{bac}_f(\mathrm{DOC} - T_{\mathrm{BacDOC}})}{\mathrm{DOC} - T_{\mathrm{BacDOC}} + H_{\mathrm{BacDOC}}} + \frac{\partial}{\partial z}\left[K(z)\frac{\partial \mathrm{DOC}}{\partial z}\right]$$

where $\alpha_{(\mathrm{Ps,Bac,SP})} = 1 - \alpha_{\mathrm{MizSP}} - r_{\mathrm{MizA}} - (e_{\mathrm{MizPs}}, e_{\mathrm{MizBac}}, e_{\mathrm{MizSP}})$

$$\frac{\partial \mathrm{Bac}}{\partial t} = \mu_{\mathrm{Bac}}(T)e_{\mathrm{Bac}}\mathrm{Bac}\left[\frac{\mathrm{bac}_f(\mathrm{DOC} - T_{\mathrm{BacDOC}})}{\mathrm{DOC} - T_{\mathrm{BacDOC}} + H_{\mathrm{BacDOC}}} + \frac{(1 - \mathrm{bac}_f)(\mathrm{SP} - T_{\mathrm{BacSP}})}{\mathrm{SP} - T_{\mathrm{BacSP}} + H_{\mathrm{BacSP}}}\right] - g_{\mathrm{Miz}}(T)\mathrm{Miz}\frac{\mathrm{Bac}/H_{\mathrm{MizBac}}}{1 + F_{ts}} - m_{\mathrm{Bac}}\mathrm{Bac} + \frac{\partial}{\partial z}\left[K(z)\frac{\partial \mathrm{Bac}}{\partial z}\right]$$

Nutrient

$$\frac{\partial \mathrm{NH}_4^+}{\partial t} = \mu_{\mathrm{Bac}}(1 - e_{\mathrm{Bac}})\mathrm{Bac}\left[\frac{\mathrm{bac}_f(\mathrm{DOC} - T_{\mathrm{BacDOC}})}{\mathrm{DOC} - T_{\mathrm{BacDOC}} + H_{\mathrm{BacDOC}}} + \frac{(1 - \mathrm{bac}_f)(\mathrm{SP} - T_{\mathrm{BacSP}})}{\mathrm{SP} - T_{\mathrm{BacSP}} + H_{\mathrm{BacSP}}}\right] + m_{\mathrm{Bac}}\mathrm{Bac} + g_{\mathrm{Mez}}(T)r_{\mathrm{MezA}}\mathrm{Mez}\frac{F_{tl}}{1 + F_{tl}}$$
$$+ g_{\mathrm{Miz}}(T)r_{\mathrm{MizA}}\mathrm{Miz}\frac{F_{ts}}{1 + F_{ts}} - \frac{\mu_{\mathrm{Pl}}Pl\mathrm{NH}_4^+/\mu_{\mathrm{Pl}}(N)}{\mathrm{NH}_4^+ + H_{\mathrm{PlA}}} - \frac{\mu_{\mathrm{Ps}}Ps\mathrm{NH}_4^+/\mu_{\mathrm{Ps}}(N)}{\mathrm{NH}_4^+ + H_{\mathrm{PsA}}} - Ntf + \frac{\partial}{\partial z}\left[K(z)\frac{\partial \mathrm{NH}_4^+}{\partial z}\right]$$

where

$$Ntf = \begin{cases} 0, & \mathrm{PAR}(z) \geq 0.1\mathrm{PAR}(0^-)_{\max} \\ \dfrac{0.1\mathrm{PAR}(0^-)_{\max} - \mathrm{PAR}(z)}{0.1\mathrm{PAR}(0^-)_{\max}}\alpha_{AN}\mathrm{NH}_4^+, & \mathrm{PAR}(z) < 0.1\mathrm{PAR}(0^-)_{\max} \end{cases}$$

$$\frac{\partial \mathrm{NO}_3^-}{\partial t} = Ntf - \frac{\mu_{\mathrm{Pl}}Pl\mathrm{NO}_3^-/\mu_{\mathrm{Pl}}(N)}{\mathrm{NO}_3^- + H_{\mathrm{PlN}}}\frac{H_{\mathrm{PlA}}}{\mathrm{NH}_4^+ + H_{\mathrm{PlA}}} - \frac{\mu_{\mathrm{Ps}}Ps\mathrm{NO}_3^-/\mu_{\mathrm{Ps}}(N)}{\mathrm{NO}_3^- + H_{\mathrm{PsN}}}\frac{H_{\mathrm{PsA}}}{\mathrm{NH}_4^+ + H_{\mathrm{PsA}}} + \frac{\partial}{\partial z}\left[K(z)\frac{\partial \mathrm{NO}_3^-}{\partial z}\right]$$

T_{BacDOC}: refractory DOC (800 mg C m^{-3}); T_{BacSP}: refractory particles (5 mg C m^{-3}); $\mathrm{PAR}(0^-)_{\max}$: PAR maximum at sea surface water.

where A is an empirical constant (0.25; Oakey 1982); ε_w and ε_c are the dissipations of turbulent kinetic energy generated by winds and currents, respectively; k is the von Karman's constant (0.4); ρ_w is the density of sea water (sigma-t data); ρ is a reference density (10^3 kg m^{-3}); g is the gravitational acceleration; and ν is the kinematic viscosity (1.3×10^{-6} m^2 s^{-1}; Yoshida and Oakey 1996). The friction velocity (ω_*) is given by (Wu 1982)

$$\omega_*^2 = \frac{\rho_a}{\rho_w} C_D U_{10}^2 \tag{9}$$

with

$$C_D = (0.8 + 0.065U_{10}) \times 10^{-3}$$

where ρ_a is the air density, C_D is the drag coefficient, and U_{10} is the wind speed at 10 m above the sea surface (all values are in MKS units). The linear increase in C_D with wind speed holds for wind speeds up to 25 m s^{-1} (Smith 1988), which are never reached in our time series (*see Fig. 1*). We did not calculate du/dz explicitly as a function of tide and baroclinic current but instead estimated it from the standard deviation of current-meter velocities recorded at 110 m during the study. This is used only as a means to provide an additional constant level of mixing energy to reproduce the observed mixed layer and adjusted accordingly.

Vertical mixing is limited in the pycnocline. In the open ocean, $K(z)$ in the pycnocline is on the order of 1×10^{-5} m^2 s^{-1} (Ledwell et al. 1993). Given higher mixing energy in coastal waters than in the open ocean (e.g., tides), $K(z)$ in the pycnocline was assigned to be 3×10^{-5} m^2 s^{-1} (Toro 1992). In the model, the pycnocline is detected by a gradient Richardson number (Ri) higher than 0.25:

$$0.25 < \mathrm{Ri} = \frac{\dfrac{g\partial\rho_w}{\rho\partial z}}{\left(\dfrac{\partial u}{\partial z}\right)^2} \tag{10}$$

with

$$\frac{\partial u}{\partial z} = \left(\frac{\partial u}{\partial z}\right)_w + \left(\frac{\partial u}{\partial z}\right)_C$$

where $(\partial u/\partial z)_w$ and $(\partial u/\partial z)_c$ are shears generated by wind and currents, respectively (Price et al. 1986) and wind shear is calculated as $(\partial u/\partial z)_w = \omega_*/kz$. Below the pycnocline, only current dissipation of turbulent kinetic energy was taken into account.

During late fall and winter time, the mixed-layer depth increases due to stronger winds and relatively dense waters produced from cooling at the surface. Following Denman and Gargett (1983) and Archer (1995), when air temperature is lower than that of surface waters and ice forms, a convective equivalent eddy diffusivity K_{zc} (in m^2 d^{-1}) is added based on the observed mixed-layer depth D (m) and a proportionality coefficient ($\alpha_{kzc} = 1.25 \times 10^{-5}$):

$$K_{zc} = \alpha_{kzc} \times D \tag{11}$$

This is admittedly a rough approximation to the convective equivalent eddy diffusivity, but it allows production of nitrate profiles close to those observed at the end of winter.

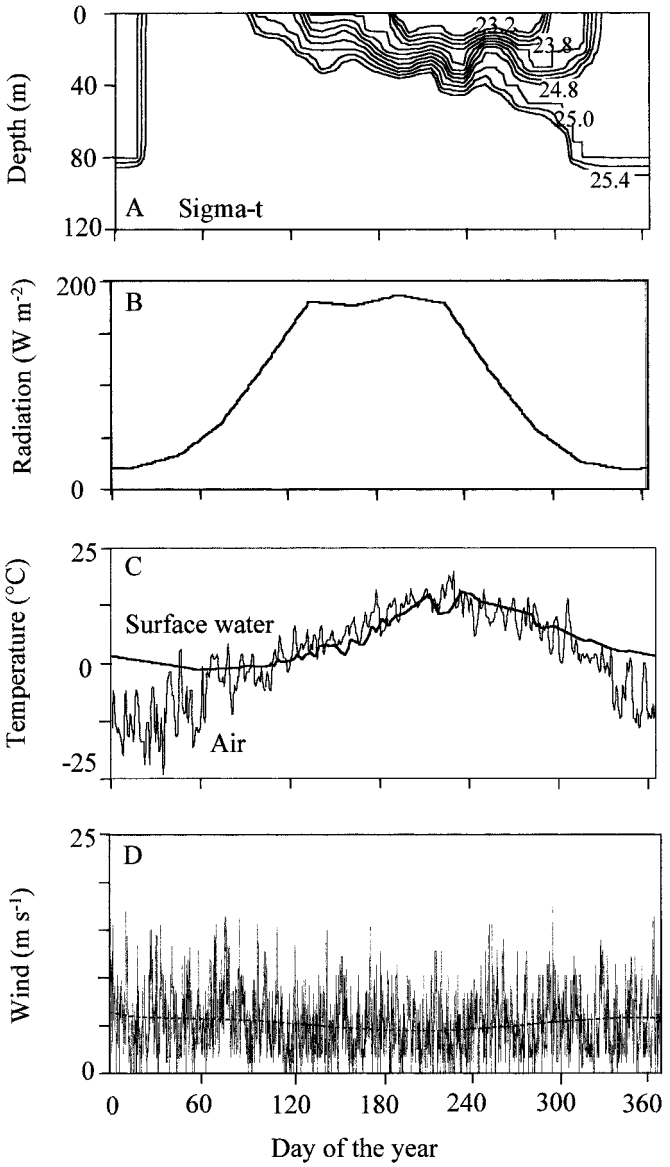

Fig. 1. Forcing variables used in the simulation. (A) Depth-time isolines of sigma-t from field measurements; (B) solar radiation from satellite observations; (C) daily mean air and surface water temperature; (D) hourly mean wind speed with polynomial trend (smoothed line).

Parameter estimation—We used the method of Prunet et al. (1996), to which readers are referred for a detailed description, to optimize the fit between simulations and observations. Briefly, the cost function

$$F(\mathbf{p}) = \sum_{j=1}^{m} [d_j - c_j(\mathbf{p})]^2 \tag{12}$$

is minimized by the Gauss-Newton linear iterative method ($\mathbf{p}$ is the parameter set $p_1, \ldots, p_n$; m is the number of measurements; d is the observed data; c is the modeled value). First, a gradient matrix is obtained by perturbing each parameter in turn from a control run (the simulation with initial parameter values prior to parameter estimation)

$$\mathbf{A}_j^{*i} = \frac{\partial c_j}{\partial p_i} = \frac{c_j(\mathbf{p} + \delta p_i) - c_j(\mathbf{p})}{\delta p_i} \quad (13)$$

where i is the parameter index and j is the data index. Then $\mathbf{A}^*$ is normalized by diagonal matrices of data errors and parameter variances

$$\mathbf{A} = \mathbf{W}^{1/2}\mathbf{A}^*\mathbf{S}^{1/2}, \quad \text{with } W_j^j = 1/\zeta_j^2 \quad \text{and} \quad S_i^i = \sigma_i^2 \quad (14)$$

where ζ_j is the error of d_j and σ_i is the a priori variance of parameter p_i. Normalization by parameter variances eliminates distortions due to their different units. Parameter variances σ_i are estimated from the literature and from previous modeling experiments.

Starting from an initial set of parameter values, the method iterates through modifications of these parameters until the cost function converges. Parameter modifications at each iteration were calculated by solving the following equation:

$$d\mathbf{p} = \mathbf{A}^{-1}\mathbf{W}^{1/2}(\mathbf{d} - \mathbf{c}) \quad (15)$$

where $\mathbf{d}$ and $\mathbf{c}$ are the vectors of observed and modeled data, respectively. Singular value decomposition was used to compute the inverse of $\mathbf{A}$ to prevent numerical instabilities (*see* Prunet et al. 1996 for details). These parameter modifications were continued until the difference in total root mean square error (rmse)

$$\text{rmse} = \sqrt{\frac{1}{m}\sum_{j=1}^{m}\frac{(d_j - c_j)^2}{\zeta_j^2}} \quad (16)$$

between two successive iterations was below 10^{-3}. Annual model cycles were run repeatedly with this modified parameter set until all state variables were in annual balance. This caused changes in the initial conditions, and the data assimilation process was conducted again until both initial conditions and parameters are stable. Only the initial concentrations of nitrate changed noticeably following these adjustments.

Parameter estimation was conducted from two different control runs. One is the parameter set used in Tian et al. (2000), called the JGOFS control run. The other is a parameter set modified by trial and error to simulate the Bonne Bay data, called the BB control run. The final parameter sets obtained after the fitting process are called the JGOFS and BB solutions, respectively.

With complex, highly nonlinear models, there is no straightforward procedure to gauge the importance of parameters in controlling the solution. Computing estimates of parameter error and resolution is numerically very costly and is valid only if the response surface of the cost function (sensitivity to parameter changes) approximates a parabola. Taking advantage of the fact that we are working from two initial parameter sets, we calculated two diagnostics for each parameter: (1) the absolute change from initial to final value, normalized to the initial value (percent change), and averaged between solutions (pch)

$$\text{pch} = \frac{\left|(p_{\text{BB}}^0 - p_{\text{BB}}^f)/p_{\text{BB}}^0\right| + \left|(p_{\text{JGOFS}}^0 - p_{\text{JGOFS}}^f)/p_{\text{JGOFS}}^0\right|}{2}100 \quad (17)$$

where the superscripts 0 and f refer to the initial and final parameter estimates, respectively, and (2) the difference between the final estimates for the two solutions, normalized to the average of the final estimates (pdf)

$$\text{pdf} = \frac{2\left|(p_{\text{BB}}^f - p_{\text{JGOFS}}^f)\right|}{(p_{\text{BB}}^f + p_{\text{JGOFS}}^f)}100 \quad (18)$$

We assume that the parameters that maximize pch (are changed the most from their initial estimates) and minimize pdf (converge to similar final values from different initial values) are the most important in controlling the model-data misfit. Therefore, we took the ratio of pdf to pch and ordered the parameters from the smallest value of this ratio to the largest, taking the smallest ratios as indicative of parameters that have the most important influence on the result.

Numerical procedures—The turbulent eddy diffusivity $K(z)$ was calculated with Eqs. 8–10 every hour. The convective equivalent eddy diffusivity was then added to yield the total diffusivity. The partial differential equations of the biological model were solved by finite differences. The vertical resolution (Δz) of the model is 1 m and the time step (Δt) is 1 h for biological processes. The time step to mix state variables was variable and computed by $\Delta t = 0.4\Delta z/K(z)$. The time step to advect sinking particles was determined as $\Delta t = \Delta z/s$ (s is the particle sinking velocity). Convergent and stable results were obtained by using these numerical resolutions. Constant concentration was used at the bottom boundary by considering that a steady state is reached near the bottom (120 m).

Data

Physical data—Bonne Bay is located in the northeast GSL, on the west coast of Newfoundland. The Bonne Bay station (49°32′N, 57°56′W) was occupied from March to September 1991. Temperature and salinity profiles were obtained every 3 d by using a CTD instrument (Seabird™) during the sampling year. For winter (December–February), four CTD profiles conducted in 1992 and 11 historical profiles from the Maurice Lamontagne Institute (MLI) archive were used. Sigma-t distribution determined from CTD profiles shows that waters remained stratified in early winter, at about 100 m (Fig. 1A). From late January through early April, the whole water column was homogeneous without noticeable stratification. Stratification developed in late April and stabilized near the surface until early autumn, when it began to deepen and reached ca. 100 m in late autumn. A constant current shear (4×10^{-3} s^{-1}) was used in the calculation of diffusivity. Data for all-sky shortwave radiation were interpolated from monthly mean values between 1985 and 1989 based on satellite measurements (http://ingrid.ldgo.columbia.edu; Fig. 1B). Temperature in surface waters (CTD data) ranged from −1.5°C in winter to 15.5°C in August (Fig. 1C). Air temperature varied between −24°C and 20°C (Fig. 1C), and hourly wind speed varied between 0 and 24 m s^{-1}, with stronger average speeds in late autumn and winter than in summer (Fig. 1D).

Biological data—Large (>5 μm) and small phytoplankton (<5 μm) biomass, primary production, microzooplank-

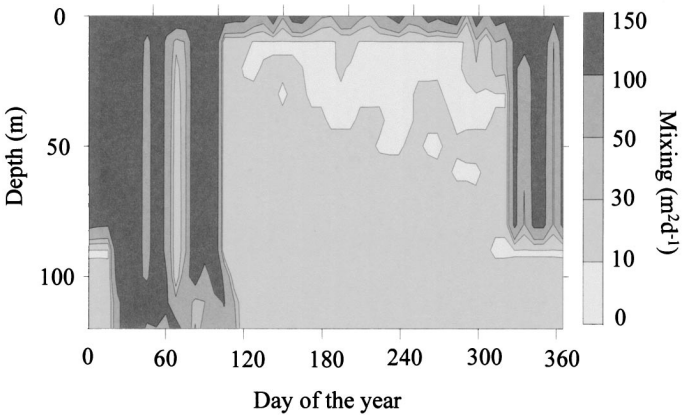

Fig. 2. Depth-time distribution of vertical mixing coefficient (turbulent eddy diffusivity) generated by the diagnostic physical model based on CTD profiles and wind and air temperature data.

ton biomass, and nitrate concentrations were measured from water samples collected at 10 standard depths (0, 2.5, 5, 10, 15, 20, 30, 40, 60, and 100 m). For phytoplankton biomass, samples were filtered with 0.7-μm Whatmann GFF and 5-μm Nucleopore polycarbonate filters. Filters were next soaked in 90% acetone during 24 h in the dark at 0°C, and chlorophyll *a* (Chl *a*) concentrations were determined with a Turner Designs Fluorometer calibrated against pure Chl *a* extract (Strickland and Parsons 1972). Phytoplankton carbon was then estimated with a carbon/Chl *a* ratio, 61 for large cells and 80 for small cells resulted in the final BB solution.

Primary productivity was measured in situ with the ^{14}C method (Strickland and Parsons 1972). Triplicate subsamples were inoculated with $Na_3{}^{14}CO_3$ and incubated in situ for 3–4 h between 1200 and 1800 h. The incubated samples were filtered with 0.4-μm Nucleopore filter, and the filters were then placed in scintillation vials and acidified to remove inorganic carbon. Then, 10 ml ACS scintillation fluor were added and the ^{14}C radioactivity was measured with an LKB™ liquid scintillation counter. Hourly primary production rates were calculated from disintegrations per minute counts. Daily primary production was obtained based on daily total irradiance and hourly production.

Microzooplankton abundances were determined by phase-contrast inverted microscopy from lugol-preserved samples (Lund et al. 1958). Microzooplankton abundances were converted to carbon biomass by using the C : volume relationship of Putt and Stoecker (1989). Nutrient concentrations were analyzed with a Technicon auto-analyzer. Mesozooplankton were sampled by vertical hauls from 0 to 100 m with a WP2™ net of 100-μm mesh size equipped with a flowmeter. Two aliquots from each zooplankton haul were dried and combusted (500°C for 24 h) to obtain values for ash-free dry weight (AFDW). Zooplanktonic POC was estimated to be 50% of AFDW.

Primary production, nitrate concentrations, phytoplankton, and microzooplankton biomass were integrated over the euphotic zone and used to constrain the model (42 time points with 262 integrated estimates). Because mesozooplankton exhibit diel vertical migration, model-measurement calibration was conducted on integration over the top 100 m of the water column.

Sinking fluxes of organic matter at 90–100 m (10–20 m above the bottom) were estimated by using consecutive short-term (2–4 d) deployments of three single sediment traps set approximately 100 m apart in a triangular pattern (*see* Starr et al. 1994 for details). Traps were Plexiglas cylinders 10-cm diameter and 40–43 cm high. The traps were attached to polyester cables moored on the bottom with an anchor weight and kept vertical by surface buoys. During retrieval, traps were closed with a messenger release system. The settled particles were collected on Whatman GFF filters for the determination of particulate organic carbon and nitrogen by using a Perkin-Elmer 240 Elemental CHN analyzer.

The coefficient of variation between traps was of the order of 22% during the sampling year. In spite of the fact that no poison or fixative was used in the sediment traps, the decomposition of settled matter should be weak and constant throughout the sampling period as the temperature conditions surrounding the traps were quite stable, ranging between −0.5°C and 0.5°C. Moreover, no seasonal pattern in the POC/PON ratio of the settled material was observed. POC/PON ratios >10, which often characterize resuspension periods in coastal areas, were not found throughout the sampling period. Consequently, the present data are probably close to net sedimentation rates.

Results

Water column mixing—Values generated by the physical model ranged from 3 to 150 $m^2\ d^{-1}$ (Fig. 2A). At the beginning of the year, the model generated strong mixing in the upper 80 m ($K(z) > 100\ m^2\ d^{-1}$) and low mixing coefficients below the pycnocline. From mid-January until mid-April, the water column was completely mixed, interspersed with short periods of reduced mixing. From mid-April to mid-November, vertical mixing was limited, except for the

Table 4. Root mean square errors between observations and simulations (rmse) for all observations (Total) and broken down by type of observation. TP, total phytoplankton (literature values for late fall); PP, primary production; SF, sinking flux. Other state variables are defined in Table 1. The last row gives the difference in rmse between the two solutions normalized to the mean rmse.

Run	Total	TP	*Pl*	*Ps*	PP	Mez	Miz	SF	NO_3^+
JGOFS control	112	72	60	187	111	55	180	17	19
JGOFS solution	50	19	61	55	88	51	41	9	17
BB control	107	38	200	58	113	154	38	13	22
BB solution	50	39	67	58	88	41	40	11	17
Div/Mean	0	0.69	0.09	0.05	0	0.22	0.02	0.20	0

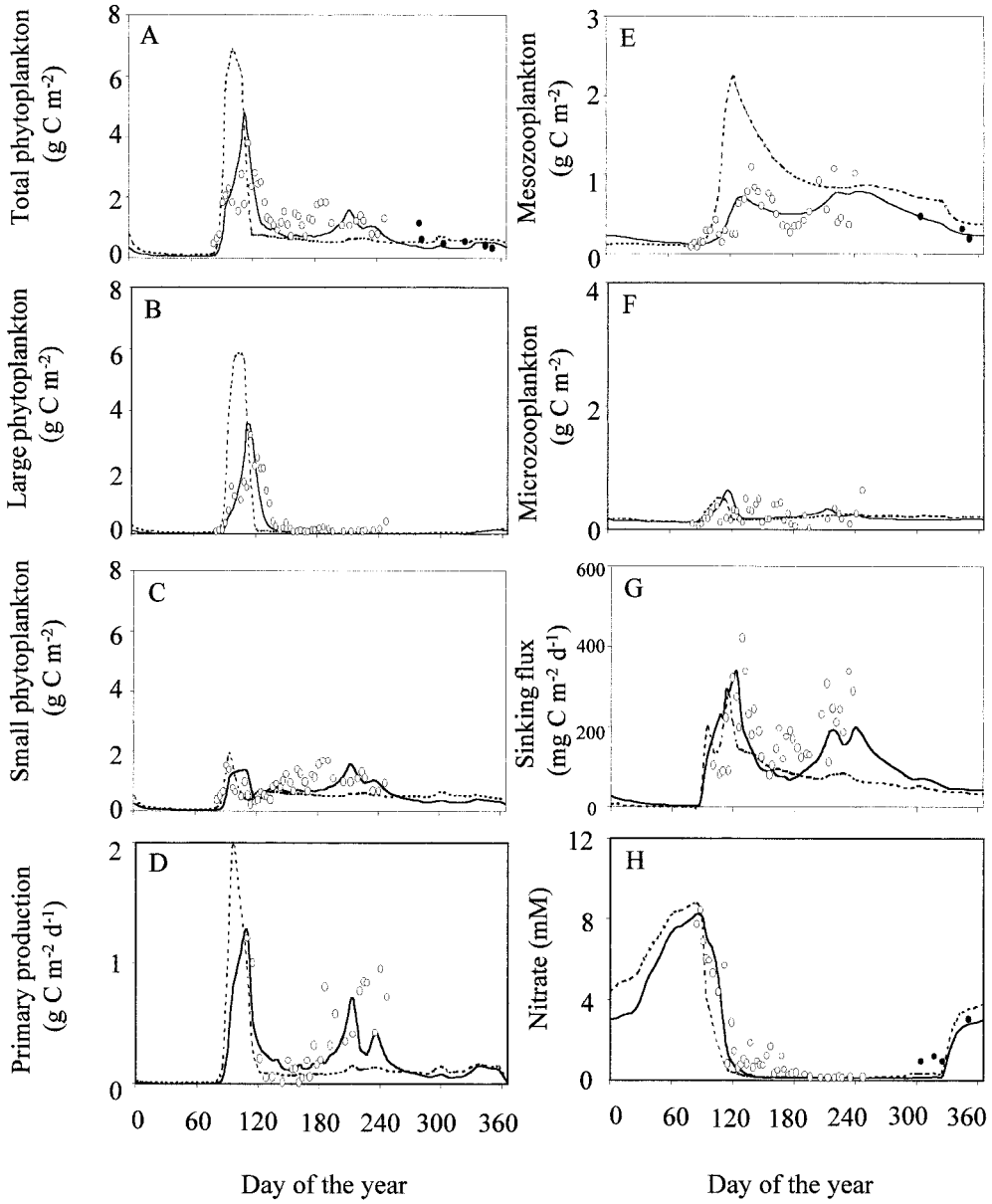

Fig. 3. Model simulations of data from the 1991 Bonne Bay time series. Dotted lines are the Bonne Bay control run; solid lines are the final solution obtained after parameter estimation; open circles are data collected in 1991; and closed circles are data from previous studies.

top 10 m characterized by high and variable turbulent eddy diffusivities. After mid-November, the model responded to the decrease in air temperature and increase in wind stress by producing strong vertical mixing down to 80 m from mid-fall until the end of the year.

Observed biological seasonal cycles—The seasonal cycle observed in Bonne Bay during 1991 (Fig. 3) is typical of high-latitude ecosystems. There was a strong spring bloom following ice-out dominated by large phytoplankton and accompanied by a rapid decline in nitrate levels in the surface layer. The biomass of large phytoplankton declined to very low levels during summer, while that of small phytoplankton was maintained at approximately constant values and consequently became dominant during the summer oligotrophic period. Mesozooplankton biomass rose and fell with the spring bloom, and there was a hint of a secondary maximum in July–August. Microzooplankton biomass was also fairly stable throughout the season. All this agrees with a change from a large-sized food web in spring to a microbial food web in summer driven by the seasonal cycle of mixing and stratification.

However, the sinking fluxes showed a distinctly bimodal pattern, with maxima in spring (late April–early May) and late summer (August). This corresponded roughly with the seasonal evolution of primary production, which fell to very low levels immediately after the spring bloom and rebounded from mid-June to reach a second peak in late August–

Table 5. Model parameters, their initial values, and their final values at the minimum of the cost function for the JGOFS and BB solutions. The parameters are listed in increasing order of the ratio pdf : pch, which is the percent difference between the final parameter estimates (pdf) divided by the percent changes from the initial to the final value, averaged between the two solutions (pch). A dash indicates not determined. *See the text for more details.*

Parameter	JGOFS control run		BB control run		pch	pdf	pdf : pch
	Initial	Final	Initial	Final			
DOC production of large phytoplankton	0.02	0.07	0.04	0.07	162	0	0.00
Aggregation coefficient	0.005	0.03	0.02	0.03	275	0	0.00
Maximum mesozooplankton grazing rate at 0°C	0.5	1.26	0.7	1.2	112	5	0.04
NH_4^+ from mesozooplankton respiration	0.03	0.25	0.05	0.19	507	27	0.05
Maximum growth rate of small phytoplankton at 0°C	1	0.82	1	0.83	18	1	0.07
Constant of *T* influence on *Pl* (*Ps*) growth	0.1	0.21	0.05	0.18	185	15	0.08
NH_4^+ from microzooplankton respiration	0.03	0.19	0.05	0.31	527	48	0.09
Constant of *T* influence on bacterial growth	0.1	0.36	0.21	0.31	154	15	0.10
Constant of *T* influence on MiZ growth	0.1	0.26	0.16	0.21	96	21	0.22
Half saturation of Miz predation on Bac	120	77	80	73	23	5	0.24
Maximum bacterial uptake rate at 0°C	0.5	0.3	0.24	0.33	39	10	0.25
Maximum growth rate of large phytoplankton at 0°C	0.7	0.75	1	0.78	15	4	0.27
Growth efficiency of bacteria	0.15	0.33	0.3	0.27	65	20	0.31
Half saturation of Mez grazing on *Pl*	80	89	80	86	10	3.5	0.37
Half saturation of NH_4^+ for *Ps*	0.5	0.6	0.3	0.5	44	18	0.42
DOC production of small phytoplankton	0.04	0.09	0.04	0.06	87	40	0.46
Half saturation of Miz grazing on *Ps*	120	77	80	68	26	12	0.49
Growth efficiency of Miz grazing on SP	0.26	0.32	0.3	0.3	12	6.5	0.56
Half saturation of small particles for Miz	120	120	80	200	75	50	0.67
Mortality of mesozooplankton	0.02	0.04	0.02	0.025	51	46	0.74
Growth efficiency of Mez grazing on *Pl*	0.26	0.18	0.3	0.12	46	40	0.88
Half saturation of small particles for bacteria	30	30	30	92	104	101	0.98
Growth efficiency of Mez predation on Miz	0.26	0.23	0.4	0.3	18	26	1.45
Maximum microzooplankton grazing rate at 0°C	1	1.56	1	0.94	31	50	1.60
Growth efficiency of Miz grazing on *Ps*	0.26	0.18	0.3	0.26	22	36	1.65
Half saturation of NO_3^- for *Ps*	0.5	0.7	1	1.1	25	44	1.78
Fraction of free bacteria	0.7	0.7	0.7	0.74	3	6	1.94
Small particles from feeding losses of Miz	0.3	0.34	0.3	0.26	13	27	2.00
Mortality of large phytoplankton	0.02	0.01	0.02	0.03	75	150	2.00
Half saturation of NO_3^- for *Pl*	1.0	1.1	1	0.9	10	20	2.00
Half saturation of Mez predation on Miz	80	92	80	61	20	41	2.09
C : Chlorophyl *a* in large phytoplankton	50	50	75	61	9	20	2.12
Half saturation of DOC for bacteria	150	126	150	151	9	19	2.17
DOC from feeding losses of mesozooplankton	0.4	0.14	0.3	0.3	33	73	2.24
Half saturation of NH_4^+ for *Pl*	1.0	1.1	1	0.5	30	75	2.50
Nitrification rate	0.03	0.03	0.03	0.01	34	100	3.00
Growth efficiency of Miz grazing on Bac	0.26	0.26	0.4	0.34	8	32	3.56
Constant of *T* influence on Mez growth	0.1	0.11	0.04	0.0004	55	200	3.64
C : Chlorophyll *a* in small phytoplankton	50	50	75	80	4	46	13.85
Small particles from feeding losses of Mez	0.2	0.2	0.2	0.2	—	—	—
Bacterial mortality and excretion	0.07	0.07	0.02	0.02	—	111	—
Convection-mixed layer depth relation	1.25	1.25	1.25	1.25	—	—	—
Half saturation of large particles for Mez	80	80	80	80	—	—	—
Sinking velocity of large particles	100	100	100	100	—	—	—
Breakdown coefficients of large particles	0.858	0.858	0.858	0.858	—	—	—

early September. Therefore, the data showed no obvious differences in export between the spring and late summer period, even though the latter period was dominated by small cells with relatively low biomass.

Parameter estimation—Both parameter estimation runs reduced the root mean square error (rmse) between model and data from the control simulations by over half and converged on the same rmse (Table 4). The rmse was also broken down among types of observations fitted by the models. Generally, the divergences between solutions in the observation-specific rmse (measured as the difference in rmse normalized to the averaged rmse) were small and less than 10% (Table 4). The BB solution tended to give a better fit to the mesozooplankton data at the expense of providing a poorer fit to the sinking flux numbers. However, the divergences were of the order of 20%, probably small relative to the uncertainty in the data.

For simplicity, we illustrate only the match between the BB simulations and the data (Fig. 3). Results with the

JGOFS solution are essentially the same. The initial BB control run largely overestimated the spring phytoplankton bloom. Large phytoplankton biomass, primary production, and mesozooplankton were overestimated in spring, whereas small phytoplankton biomass and primary production were underestimated in summer. Also, the control run simulates a spring peak in particle flux followed by a steady decline over the summer, whereas the observations show a second flux maximum developing during summer. All these discrepancies were corrected after the parameter estimation and the summer flux peak in particular is reproduced.

Based on the parameter indices described above (Eqs. 17 and 18), the most important and robust parameter changes needed to reproduce these patterns were substantial increases in the DOC production by large phytoplankton and in the particle aggregation coefficient (Table 5). The mesozooplankton maximum grazing rate (at 0°C) and ammonium regeneration by microzooplankton and mesozooplankton also had a strong response, and all were increased substantially from their initial values. Temperature forcings on all components of the microbial food web (small phytoplankton, bacteria, and microzooplankton) were also raised substantially. The temperature effect exponents for phytoplankton and microzooplankton were raised to ca. 0.2–0.25 in both solutions from initial values of ca. 0.1. The temperature effect exponents for bacteria were even higher, reaching ca. 0.3 in both the JGOFS and BB final solutions. The exponent for mesozooplankton in contrast ranked near the bottom in terms of response and robustness.

It is difficult to define a cutoff between important and less important parameters based on our qualitative measures. Nevertheless, this first group of parameters with pdf : pch ratios ≤ 0.20 are those that consistently combine strong changes from initial estimates with convergence between solutions (the exception is the maximum growth rate of small phytoplankton, which ranks low on this scale only because it converges on similar estimates). Parameters with ratios >0.20 appear less consistent between solutions. Using an unnormalized pdf (excluding parameters that have no change from initial to final estimate) identifies the same most sensitive parameters. Similarly, normalizing the pdf in different ways (e.g., by the change in parameter under the BB solution only) identifies the same group of sensitive parameters. Numerous sensitivity simulations with the model also confirm our identification of this subset of the parameters (results not shown). Within the constraints of this model structure, the particle flux peaks cannot be reproduced without increasing the aggregation coefficient. Also, the summer production rates can only be raised toward observed levels by simultaneously increasing the production of DOM during spring, the remineralization rates through the zooplankton, and the sensitivity of microbial rates to temperature. Combining both effects on flux and production allows the model to reproduce the summer flux maximum.

Simulated annual production and fluxes—The solutions were diagnosed by integrating the trophic flows over the euphotic zone for each simulated time step and by then summing the flows over the annual cycle and also over four 3-month seasonal periods: winter (January–March), spring (April–June), summer (July–September), and autumn (October–December). Beginning with the annual integrations (Table 6), we see that the gross inputs and outputs are very comparable between the solutions. Both solutions produce a closed mass balance with upward nitrate fluxes (converted to carbon equivalents) balancing the sum of sinking fluxes and mixing losses of DOC and POC. Sinking fluxes account for ca. 60% of the total export, and mixing losses account for the remainder, with equal shares from DOC and POC. Primary production is ca. 150 g C m^{-2} yr^{-1}, and the *f*-ratio (ratio of nitrate-based to total production) is ca. 0.38. The export ratio (*e*-ratio) calculated from sediment traps is substantially lower than the *f*-ratio on an annual basis.

Table 6. Annual biological production and fluxes of the two final simulations (g C m^{-2} yr^{-1}). The last column (Div/Mean) is as in Table 4.

	JGOFS	BB	Mean	Div/Mean
Nitrate flux	55	56	56	0.02
Sinking flux	33	36	35	0.09
DOC mixing export	11	8	10	0.3
POC mixing export	11	12	12	0.08
Primary production	152	143	148	0.6
f-ratio	0.36	0.39	0.38	0.08
e-ratio	0.22	0.25	0.24	0.125
Large phytoplankton	36	22	29	0.48
Small phytoplankton	116	121	119	0.04
Mesozooplankton	12	6	9	0.67
Microzooplankton	29	19	24	0.42
Bacteria	27	21	24	0.25

Breaking down the production rates by compartment reveals more discrepancies between the solutions (Table 6). In general, the production rates are higher for the JGOFS solution than for the BB solution. Even though the solutions give comparable fits to the biomass numbers, the simulated turnover rates can be different by a factor of 2 for mesozooplankton and less for the other compartments.

Simulated seasonal flow networks—Only the seasonal integrations for the Bonne Bay (BB) simulations for the spring and summer periods are shown here (Fig. 4). The JGOFS flow networks are qualitatively similar and lead to broadly the same interpretations. Also, only the spring and summer periods are constrained by data. As mentioned earlier, the model generated balanced nitrate upward flux and carbon export on an annual basis. However, the simulated seasonal networks are not balanced. During spring, only 39% of the new production is exported by gravitational sinking, 21% is mixed down into the subeuphotic zone as DOM and detritus, and the remainder is retained within the euphotic zone. During summer, the nitrate upward flux accounts for 50% of the particle sinking flux and ca. 40% of the total carbon export. In contrast with spring, when only part of new production is exported, carbon export in summer exceeds new production. In fact, approximately half of the summer carbon export originates from regenerated production.

The model simulated the expected seasonal shifts in food web structure and trophic flows from essentially a nitrate-based herbivorous food web during spring to an ammonium-

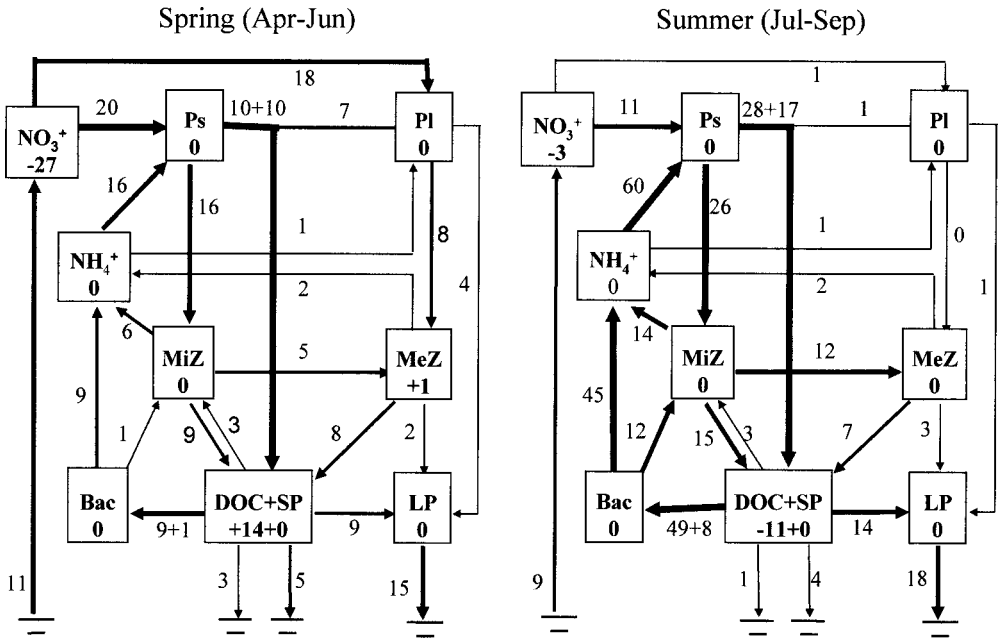

Fig. 4. Simulated spring and summer food web trophic flows in the euphotic zone from the BB final solution. The values of state variables represent the net budgets and that between them are gross flows in g C m^{-2} integrated over the corresponding season. Ammonium and nitrate are given in carbon equivalents.

based microbial food web during summer (Fig. 4). There is also a large simulated DOM production during spring, with only half of it removed during the same period, either by bacterial use or by vertical mixing. The remainder accumulates in the euphotic zone and is used during the summer. This use leads to a strong increase in bacterial production and in ammonium remineralization, which then fuels production by small phytoplankton. This enhances the production of microzooplankton and in turn the microzooplankton–mesozooplankton trophic link. However, this microbial link from bacterial/small phytoplankton production to mesozooplankton and then to fecal pellets contributes only a minor share of the summer flux. Coagulation/aggregation are in fact the major mechanisms leading to large sinking particles, accounting for 60% of the sinking flux in spring and 78% in summer (Figs. 4–5). The direct flux of large phytoplankton is important only during the spring bloom, whereas that of fecal pellets, although increasing slowly during the summer, remains low throughout the entire annual cycle.

Discussion

Export fluxes in mid- to high-latitude systems often show much smaller seasonal variations than new production (Rivkin et al. 1996; Smith and Dunbar 1998). The processes responsible for this pattern remain poorly understood. Shifts in food web structure are generally expected to generate strong variations in export. Rivkin et al. (1996) proposed an alternate model where shifts in food web structure actually act to stabilize the export flux over the seasonal cycle. Our model simulations of the 1991 time series of particle sinking flux in Bonne Bay point to other processes that may be more determinant. One is that upward nitrate fluxes and new production may be much more evenly distributed over the annual cycle than is generally supposed or inferred from observed changes in nutrient levels in surface waters. Another is that delayed remineralization of suspended detritus and DOM arising from the spring bloom may be a significant process linked in some fashion to seasonal temperature changes. Finally, the formation of large fast-sinking particles may be dominated by physico-chemical processes of coagulation and aggregation during the whole year and not by shifts in food web structure. These findings have major implications for our views on carbon and nutrient cycles in the surface layer and on the need to represent them properly in biogeochemical models. The strength of these conclusions, however, rests on the biological and chemical realism of the parameter estimates and also on the validity of our assumptions, mainly the one-dimensional approximation to this system.

It is evident that a fjord like Bonne Bay may be subject to lateral advective effects that are not explicitly accounted for in this model. Runoff from the drainage basin may supply nutrients and dissolved organic matter to the fjord. However, freshwater discharge into Bonne Bay is quite limited, $<0.5\%$ of the water volume annually. Given that the salinity in surface waters varies in a narrow range from 28 to 32 practical salinity units (p.s.u.), runoff has little influence in Bonne Bay and the fjord is located well away from the part of the GSL influenced by the freshwater outflow from the St. Lawrence River. Spatial sampling done during the time series work (data not shown) indicates that horizontal gradients in physical, biological, and chemical properties within the fjord and adjacent GSL regions are quite weak, so that

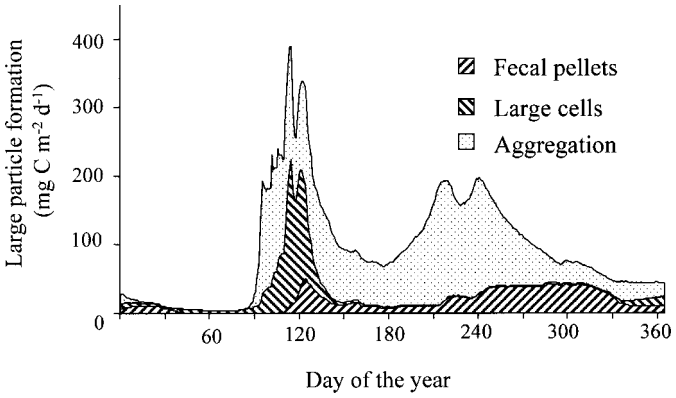

Fig. 5. Contributions of fecal pellets, large phytoplankton senescence/mortality, and physico-chemical aggregation to the formation of the large particles that constitute the sinking flux (integrated over the upper 50 m).

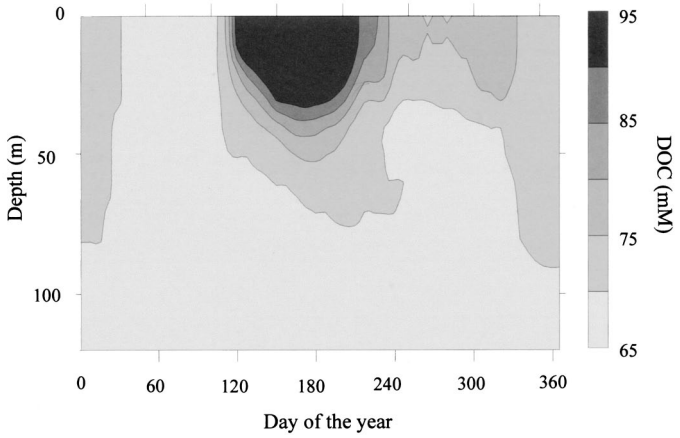

Fig. 6. Simulated seasonal cycle of DOC in the water column (from the BB final solution).

tidal exchange would not contribute important net changes at the fixed station modeled here.

Given that advective effects are small, we can look at other implications of the modeled results to assess their plausibility. The model used 3-day salinity and temperature records and hourly wind data to describe high-frequency fluctuations in vertical mixing during the stratified period. Combined with an empirical description of convective overturn during late fall and winter, our analysis reveals that the nitrate flux into the euphotic zone is spread rather evenly over the entire year. The largest share of the flux occurs during winter, yet that accounts for only 37% of the annual flux. Autumn, spring, and summer fluxes account for 27, 20, and 16% of the annual value, respectively. This agrees with other estimates of the seasonal distribution of nitrate supply. For example, Michaels et al. (1994) demonstrated that only one quarter to one third of the annual nitrate requirement was supplied during winter convection at the Bermuda time series. Other studies have emphasized the role of wind fluctuations in generating high nitrate fluxes under stratified conditions (Klein and Coste 1984). Fluctuations in wind stress most likely contributed significantly to the nitrate flux into the euphotic zone during summer.

Transient wind-driven upwelling events are common in the northern Gulf of St. Lawrence during summer (Rose and Leggett 1988), as is the case in other mid- to high-latitude coastal seas (Edwards et al. 1996). These events can inject nutrients into the euphotic zone (Haapala 1994) and enhance phytoplankton biomass and primary production (Takahashi et al. 1986). The high-frequency CTD data captured vertical displacements of the thermocline during the summer 1991 in Bonne Bay. The most important displacement was the raising of the thermocline between day 203 and 230, probably due to an upwelling generated by southerly alongshore winds (Gilbert and Pettigrew 1993). Indeed, the nitrate flux increased significantly during this period. The estimated monthly integrated nitrate flux was 15 mmol N m^{-2} in June, while it increased to 29 and 42 mmol N m^{-2} in July and August, respectively. If the flux in June is considered as a background unaffected by upwelling, the displacement of the thermocline from day 203 to 230 upwelled 41 mmol nitrate to the euphotic zone, i.e., 3.3 g C m^{-2} in carbon equivalents and accounting for 37% (3.3/9) of the summer nitrate flux.

Our data and analyses reveal the difficulty in assessing the role of trophic or other processes in controlling seasonal patterns in export without first accounting for high-frequency and mesoscale physical events. Platt and Harrison (1985) have used the nonlinear nature of new production variability to show that underestimation of the natural variability leads to underestimation of nutrient fluxes and new production. Since then, a number of studies with physical-biological models have confirmed that model estimates of primary and new production are very sensitive to the vertical and temporal resolution of the description of the physical environment (Bissett et al. 1994). Estimates of those fluxes degrade rapidly as the description becomes coarser. Legendre and Rassoulzadegan (1996) developed a theory by which the export ratio varies with the frequency and intensity of mixed-layer variations. Our study extends these findings toward explaining part of the relative lack of seasonality in export observed at middle and high latitudes.

However, the summer nutrient flux only accounts for half of the summer export; the remainder is driven by remineralization or removal of materials stored in the water column from the previous spring bloom. The model simulates a seasonal increase in euphotic zone DOC of 20 mmol C m^{-3} between the prebloom winter minimum (late March) and the beginning of the postbloom summer period (early June, Fig. 6). This value seems to be relatively high compared to that observed over comparable periods at Bermuda (10 mmol C m^{-3}; Carlson et al. 1994) and the NW Mediterranean (15 mmol C m^{-3}; Copin-Montégut and Avril 1993). The three ecosystems are different, however. Surface temperature is 28°C at Bermuda in summer (Carlson et al. 1994), 21°C in the NW Mediterranean (Tian et al. 1996) and 15°C in Bonne Bay. If DOM remineralization via bacterial activities is influenced by temperature, DOM accumulation can be expected to be more important in cold seas than in warm regions. Up to 80 mmol C m^{-3} of DOM accumulation in surface waters was observed in a Norwegian fjord (Børsheim et al. 1999). Given the same order of magnitude

of DOM accumulation observed in other regions, the modeled results appear to be plausible.

The processes responsible for the seasonal accumulation and removal of DOM remain a subject of active research. One major change resulting from parameter estimation is that DOC release from phytoplankton was increased two to threefold to 0.07 d^{-1}. Recent experimental results indicate that large amounts of DOM are released from nutrient-stimulated phytoplankton blooms (Søndergaard et al. 2000). Field-based estimates of the DOC release rate constant cover a wide range, for example, 0.02–1.9 d^{-1} in the Mediterranean (Agusti et al. 1998) and 0.08 d^{-1} for Conception Bay (East Coast of Newfoundland) (Pomeroy et al. 1991). Thus, a crucial source term for the DOC accumulation produced by the model appears to be realistic.

The use of the produced material will depend on any number of potential factors constraining bacterial activity. The model generates the needed cycle of accumulation/remineralization by strongly linking microbial activity to temperature. The Q_{10} (increase in activity over a 10°C temperature range) implied by the final model solutions range from 22 to 36 for bacteria, much higher than the Q_{10} measured for bacterial growth in the field, i.e., 13 from the Arctic Ocean (Yager and Deming 1999) and five from Conception Bay (Pomeroy and Deibel 1986). However, our results qualitatively agree with the recent observation that DOC use by bacteria (and respiration) is much more sensitive to temperature than growth rate (Rivkin and Legendre 2001). Therefore, a different model parameterization that makes uptake dependent on temperature but not growth would tend to produce disproportionate increases in remineralization as temperatures rise, the result that the model is trying to reproduce by increasing the temperature sensitivity of uptake. Other factors contribute to slowing down the breakdown of labile organic materials: nutrient deficiency (Rivkin and Anderson 1997), top-down control of bacteria (Sanders et al. 1992), a combination of nutrient and top-down control (Thingstad et al. 1997), and suppression of bacterial activity by low temperatures (Pomeroy and Deibel 1986). Also, the lability of DOM will change over time due to several physico-chemical processes (Keil and Kirchman 1994; Schuster et al. 1998). It is likely that temperature in our model acts as a surrogate for a number of complex reactions that remain to be unraveled.

The minor contribution of fecal pellets in the formation of large sinking particles is due to low trophic efficiency from the microbial food web to mesozooplankton. In model simulations, the flow from microzooplankton to mesozooplankton is only 9% of the flow into the microbial food web (small phytoplankton production plus bacterial carbon demand), and only 2% of these microbial flows is channeled to large sinking particles through food web transfers (Fig. 4). Field measurements in Belgian coastal waters revealed that the trophic efficiency of the microbial food web is only 1.6% (Rousseau et al. 2000). Large phytoplankton in spring has a higher trophic efficiency than the microbial food web, but is still restricted to 44%. That a great part of primary production is not processed by zooplankton grazing is a result that also falls out from statistically constrained mass balance analyses of trophic flows (Vézina and Savenkoff 1999). Walsh (1983) developed a number of carbon budgets for shelf systems and argued from the results that roughly half of phytoplankton production suffers natural mortality. Therefore, our estimates of low trophic efficiency from the model are not at variance with other model calculations and with recent observational work.

On the other hand, our model revealed the strong role of aggregation processes in generating large fast-sinking particles throughout the seasonal cycle, particularly in summer when the microbial food web dominates. Usually, particle aggregation processes are viewed as limited to the end of bloom periods when particle concentrations are high and physiological changes in phytoplankton, particularly diatoms, make them more sticky and likely to aggregate (Jackson 1990). Transparent exopolymeric particles (TEP) can also coagulate into larger fast-sinking aggregates (Logan et al. 1995). Furthermore, TEP abundances in a comparable midlatitude system (Kattegat sound) show two peaks: one during the spring bloom and one during summer (Mari and Burd 1998). It is plausible then that physico-chemical aggregation processes are important when the herbivorous and microbial food webs mature (spring and late summer) and produce abundant material for coagulation. This modeling analysis then suggests that physical mixing processes and physico-chemical aggregation processes are at least as important as shifts in food web trophic pathways in explaining the relative constancy of export flux in mid- to high-latitude marine systems.

References

AGUSTI, S., M. P. SATTA, M. P. MURA, AND E. BENAVENT. 1998. Dissolved esterase activity as a tracer of phytoplankton lysis: Evidence of high phytoplankton lysis rates in the northwestern Mediterranean. Limnol. Oceanogr. **43:** 1836–1849.

ARCHER, D. 1995. Upper ocean physics as relevant to ecosystem dynamics: A tutorial. Ecol. Appl. **5:** 724–739.

BISSETT, W. P., M. B. MEYERS, J. J. WALSH, AND F. E. MÜLLER-KARGER. 1994. The effects of temporal variability of mixed-layer depth on primary productivity around Bermuda. J. Geophys. Res. **99:** 7539–7553.

BØRSHEIM, K. Y., S. M. MYKLESTATD, AND J. A. SNELI. 1999. Monthly profiles of DOC, mono- and polysaccharides at two locations in the Trondheimsfjord (Norway) during two years. Mar. Chem. **63:** 255–272.

BOYD, P., AND P. NEWTON. 1995. Evidence of the potential influence of planktonic community structure on the interannual variability of particulate organic carbon flux. Deep-Sea Res. **42:** 619–639.

CARLSON, C. A., H. W. DUCKLOW, AND A. F. MICHAELS. 1994. Annual flux of dissolved organic carbon from the euphotic zone in the northwestern Sargasso Sea. Nature **371:** 405–408.

COPIN-MONTÉGUT, G., AND B. AVRIL. 1993. Vertical distribution and temporal variation of dissolved organic carbon in the North-Western Mediterranean Sea. Deep-Sea Res. **40:** 1963–1972.

DENMAN, K. L., AND A. E. GARGETT. 1983. Time and space scales of vertical mixing and advection of phytoplankton in upper ocean. Limnol. Oceanogr. **28:** 801–815.

EDWARDS, A., AND OTHERS. 1996. Transient coastal upwelling and water circulation in Bantry Bay, a ria on the south-west coast of Ireland. Estuar. Coast. Shelf Sci. **42:** 213–230.

FALKOWSKI, P. G., R. T. BARBER, AND V. SMETACEK. 1998. Bio-

geochemical controls and feedbacks on ocean primary production. Science **281:** 200–206.

FASHAM, M. J. R., P. W. BOYD, AND G. SAVIDGE. 1999. Modeling the relative contribution of autotrophs and heterotrophs to carbon flow at a Lagrangian JGOFS station in the Northeast Atlantic: The importance of DOC. Limnol. Oceanogr. **44:** 80–94.

GILBERT, D., AND B. PETTIGREW. 1993. Current-meter data from Bonne Bay, Newfoundland, during the summer of 1991. Can. Data Rep. Hydrogr. Ocean. Sci. **122:** 1–63.

GRAF, G. 1992. Benthic-pelagic coupling: A benthic view. Oceanogr. Mar. Biol. Annu. Rev. **30:** 149–190.

HAAPALA, J. 1994. Upwelling and its influence of nutrient concentration in the coastal area of the Hanko peninsula, entrance to the Gulf of Finland. Estuar. Coast. Shelf Sci. **38:** 507–521.

HUNTLEY, M. E., AND M. D. G. LOPEZ. 1992. Temperature-dependent production of marine copepods: A global synthesis. Am. Nat. **140:** 201–242.

JACKSON, G. A. 1990. A model of the formation of marine algal flocs by physical and coagulation processes. Deep-Sea Res. **37:** 1197–1211.

KARL, D. M., AND OTHERS. 1996. Seasonal and interannual variability in primary production and particle flux at Station ALOHA. Deep-Sea Res. **43:** 539–568.

KEIL, R. G., AND D. L. KIRCHMAN. 1994. Abiotic transformation of labile protein to refractory protein in sea water. Mar. Chem. **45:** 187–196.

KLEIN, P., AND B. COSTE. 1984. Effects of wind stress variability on nutrient transport into the mixed layer. Deep-Sea Res. **31:** 21–37.

LEDWELL, J. R., A. J. WASTON, AND C. S. LAW. 1993. Evidence for slow mixing across the pycnocline from an open-ocean tracer-release experiment. Nature **364:** 701–703.

LEGENDRE, L., AND F. RASSOULZADEGAN. 1996. Food-web mediated export of biogenic carbon in oceans: Hydrodynamic control. Mar. Ecol. Prog. Ser. **145:** 179–193.

LOGAN, B. E., U. PASSOW, A. L. ALLDREDGE, H. P. GROSSART, AND M. SIMON. 1995. Rapid formation and sedimentation of large aggregates is predictable from coagulation rates (half-lives) of transparent exopolymer particles (TEP). Deep-Sea Res. **42:** 203–214.

LUND, J. W. G., C. KIPLING, AND E. D. LE CREN. 1958. The inverted microscope method of estimating algal numbers and statistical basis of estimation by counting. Hydrobiologia **11:** 143–178.

MARI, X., AND A. BURD. 1998. Seasonal size spectra of transparent exopolymeric particles (TEP) in a coastal sea and comparison with those predicted using coagulation theory. Mar. Ecol. Prog. Ser. **163:** 63–76.

MICHAELS, A. F., AND OTHERS. 1994. Seasonal patterns of ocean biogeochemistry at the U.S. JGOFS Bermuda Atlantic time-series study site. Deep-Sea Res. **41:** 1013–1038.

———, AND M. W. SILVER. 1988. Primary production, sinking fluxes and the microbial food web. Deep-Sea Res. **35:** 473–490.

OAKEY, N. S. 1982. Determination of the rate of dissipation of turbulent energy from simultaneous temperature and velocity shear microstructure measurements. J. Phys. Oceanogr. **12:** 256–271.

OLESEN, M., AND C. LUNDSGAARD. 1995. Seasonal sedimentation of autochthonous material from the euphotic zone of a coastal system. Estuar. Coast. Shelf Sci. **41:** 475–490.

PARKER, R. A. 1993. Dynamic models for ammonium inhibition of nitrate uptake by phytoplankton. Ecol. Model. **66:** 113–120.

PLATT, T., C. L. GALLEGOS, AND W. G. HARRISON. 1980. Photoinhibition of photosynthesis in natural assemblages of marine phytoplankton. J. Mar. Res. **38:** 687–701.

———, AND W. G. HARRISON. 1985. Biogenic fluxes of carbon and oxygen in the ocean. Nature **318:** 55–58.

POMEROY, L. R., AND D. DEIBEL. 1986. Temperature regulation of bacterial activity during the spring bloom in Newfoundland coastal waters. Science **233:** 359–361.

———, AND OTHERS. 1991. Bacterial responses to temperature and substrate concentration during the Newfoundland spring bloom. Mar. Ecol. Prog. Ser. **75:** 143–159.

PRICE, J. F., R. A. WELLER, AND R. PINKEL. 1986. Diurnal cycling: observations and models of the upper ocean response to diurnal heating, cooling and wind mixing. J. Geophys. Res. **91:** 8411–8427.

PRUNET, P., J. F. MINSTER, D. RUIZ-PINO, AND I. DADOU. 1996. Assimilation of surface data in a one-dimensional physical-biogeochemical model of the surface ocean 1. Method and preliminary results. Glob. Biogeochem. Cycles **10:** 111–138.

PUTT, M., AND D. K. STOECKER. 1989. An experimentally determined carbon: Volume ratio for marine oligotrichous ciliates from estuarine and coastal waters. Limnol. Oceanogr. **34:** 1097–1103.

RIVKIN, R. B., AND M. R. ANDERSON. 1997. Inorganic nutrient limitation of oceanic bacterioplankton. Limnol. Oceanogr. **42:** 730–740.

———, AND L. LEGENDRE. 2001. Biogenic carbon cycling in the upper ocean: Effects of microbial respiration. Science **291:** 2398–2400.

———, AND OTHERS. 1996. Vertical flux of biogenic carbon in the ocean: Is there food web control? Science **272:** 1163–1166.

ROSE, G. A., AND W. C. LEGGETT. 1988. Atmosphere-ocean coupling in the northern Gulf of St. Lawrence: Frequency-dependent wind-forced variations in nearshore sea temperatures and currents. Can. J. Fish. Aquat. Sci. **45:** 1222–1233.

ROUSSEAU, V., AND OTHERS. 2000. Trophic efficiency of the planktonic food web in a coastal ecosystem dominated by phaeocystis colonies. J. Sea Res. **43:** 357–372.

SANDERS, R. W., D. A. CARON, AND U.-G. BERNINGER. 1992. Relationships between bacteria and heterotrophic nanoplankton in marine and fresh waters: An inter-ecosystem comparison. Mar. Ecol. Prog. Ser. **86:** 1–14.

SCHUSTER, S., J. M. ARRIETA, AND G. J. HERNDL. 1998. Adsorption of dissolved free amino acids on colloidal DOM enhances colloidal DOM utilization but reduces amino acid uptake by orders of magnitude in marine bacterioplankton. Mar. Ecol. Prog. Ser. **166:** 99–108.

SMITH, S. D. 1988. Coefficients for sea surface wind stress, heat flux, and wind profiles as a function of wind speed and temperature. J. Geophys. Res. **93:** 15467–15472.

SMITH, W. O., JR., AND R. B. DUNBAR. 1998. The relationship between new production and vertical flux on the Ross Sea continental shelf. J. Mar. Syst. **17:** 445–457.

SØNDERGAARD, M., AND OTHERS. 2000. Net accumulation and flux of dissolved organic carbon and dissolved organic nitrogen in marine plankton communities. Limnol. Oceanogr. **45:** 1097–1111.

STARR, M., J. C. THERRIAULT, G. Y. CONAN, M. COMEAU, AND G. ROBICHARD. 1994. Larval release in a sub-euphotic zone invertebrate triggered by sinking phytoplankton particles. J. Plankton Res. **9:** 1137–1147.

STRICKLAND, J. D. H., AND T. R. PARSONS. 1972. A practical manual of seawater analysis. Bull. Fish. Res. Board 167 (2nd ed.).

TAKAHASHI, M., AND OTHERS. 1986. Temporal change in nutrient concentrations and phytoplankton biomass in short time scale local upwelling around the Izu peninsula, Japan. J. Plankton Res. **8:** 1039–1049.

THINGSTAD, T. F., Å. HAGSTRÖM, AND F. RASSOULZADEGAN. 1997. Accumulation of degradable DOC in surface waters: Is it caused by a malfunctioning microbial loop? Limnol. Oceanogr. **42:** 398–404.

TIAN, R. C., AND OTHERS. 1996. Iodine speciation: A potential indicator to evaluate new production versus regenerated production. Deep-Sea Res. **43:** 723–738.

———, AND OTHERS. 2000. Effects of pelagic food-web interactions and nutrient remineralization on the biogeochemical cycling of carbon: A modeling approach. Deep-Sea Res. **47:** 637–662.

TORO, C. 1992. Modélisation Diagnostique de la Circulation Tridimensionelle Induite par la Densité dans le Golfe du Saint-Laurent, Ph.D. thesis. Univ. Quebec, Rimouski.

VERITY, P. G. 1981. Effects of temperature, irradiance, and daylength on the marine diatom *Leptocylindricus danicus* Cleve. I. Photosynthesis and cellular composition. J. Mar. Exp. Biol. Ecol. **55:** 79–91.

VÉZINA, A. F., AND C. SAVENKOFF. 1999. Carbon and nitrogen flows in the surface layer of the NE Pacific. Deep-Sea Res. **46:** 2909–2939.

WALSH, J. J. 1983. Death in the sea: Enigmatic phytoplankton losses. Prog. Oceanogr. **12:** 1–86.

WU, J. 1982. Wind-stress coefficients over sea surface from breeze to hurricane. J. Geophys. Res. **87:** 9704–9706.

YAGER, P. L., AND J. W. DEMING. 1999. Pelagic microbial activity in an arctic polynya: Testing for temperature and substrate interactions using a kinetic approach. Limnol. Oceanogr. **44:** 1882–1893.

YOSHIDA, J., AND S. OAKEY. 1996. Characterization of vertical mixing at a tidal-front of George Bank. Deep-Sea Res. **43:** 1713–1744.

Received: 9 May 2000
Amended: 11 July 2001
Accepted: 24 July 2001